Journal of Alloys and Compounds 507 (2010) L26–L31

Contents lists available at ScienceDirect

Journal of Alloys and Compounds

journal homepage: www.elsevier.com/locate/jallcom

Letter

Fabrication and characterization of Lu_2O_3:Eu^{3+} nanopowders and X-ray films

N.V. Babayevskaya, T.G. Deyneka, P.V. Mateychenko, N.A. Matveevskaya, A.V. Tolmachev, R.P. Yavetskiy*

Institute for Single Crystals, STC "Institute for Single Crystals", NAS of Ukraine, 61001, 60 Lenin Ave., Kharkov, Ukraine

ARTICLE INFO

Article history:
Received 15 May 2010
Received in revised form 26 July 2010
Accepted 27 July 2010
Available online 6 August 2010

Keywords:
Lu_2O_3:Eu^{3+}
Co-precipitation
Phosphors
X-ray luminescence

ABSTRACT

Lu_2O_3:Eu^{3+} (C_{Eu} = 5 at.%) nanopowders with different particle morphology were produced via co-precipitation method using oxalic acid ($H_2C_2O_4$), ammonium hydrogen carbonate (NH_4HCO_3) and urea ($(NH_2)_2CO$) as precipitants. Lu_2O_3:Eu^{3+} films with the thickness in 20–200 μm range and relative density of 50–68 ± 2% were fabricated from the powders synthesized by painting technique. Lu_2O_3:Eu^{3+} scintillation films were characterized by SEM, XRD and luminescent spectroscopy under X-ray excitation. It was shown that films X-ray luminescence intensity depends on the oxide/polymer ratio, particle morphology and film thickness. The most effective X-ray luminescence and film homogeneity was obtained with 20 μm thick luminescent films fabricated using 100 nm spherical Lu_2O_3:Eu^{3+} nanoparticles.

1. Introduction

Active development of high-resolution X-ray imaging techniques requires new detectors with micrometer or even submicrometer spatial resolution. Oxide scintillators are considered as promising materials for high-resolution digital imaging due to high X-ray stopping power, excellent chemical stability, high conversion efficiency and high radiation hardness. Traditionally, $Bi_4Ge_3O_{12}$ [1], $CdWO_4$, $Y_2Si_2O_7$ [2] single crystals and optical ceramics [3–5] are used to convert X-rays into visible light. Despite excellent X-ray stopping power of bulk detectors, to achieve high spatial resolution they should be thinned and pixilated into arrays of pixels, thus resulting spatial resolution is limited by the pixel size (typically dozens of microns). Powder scintillation screens and thin scintillating films produced by a variety of methods are another class of materials for high-resolution X-ray detectors. $Y_3Al_5O_{12}$:Ce, $Lu_3Al_5O_{12}$:Ce [6,7] and Lu_2SiO_5:Tb films [8] grown by the liquid phase epitaxy have excellent scintillation characteristics and spatial resolution. However, film fabrication requires high quality single crystalline substrate and utilization of toxic fluxes. Dense Y_2O_3, Gd_2O_3 and Lu_2O_3 scintillating films possessing high scintillation yield can be produced via sol–gel process [9,10], but this technique is limited in terms of film thickness (hundreds of nanometers). This disadvantage was overcome in Ref. [11] where $GdTaO_4$:Tb^{3+} transparent crack-free thick films were fabricated, though their scintillation properties were not presented. Thus, relatively simple painting technique is still considered as a promising method for creation of close-packed powder X-ray screens. Improved spatial resolution of conventional screens can be achieved using nanocrystalline phosphor particles. For example, scintillation screens based on nanocrystalline Gd_2O_2S:Pr shows enhanced resolution and higher detection efficiency compared to commercially available phosphors with larger particles size when they are exposed by soft X-rays [12], that is very important for X-ray microscopy and other applications that require submicron resolution.

Just recently, a number of nanocrystalline and submicron-sized phosphors for detection of X-rays were reported: $GdAlO_3$:RE^{3+} (RE = Eu or Tb) [13], Lu_2SiO_5:Ce [14,15], $YTaO_4$:Tb [16], HfO_2:Eu [17] and Lu_2O_3:Eu^{3+} [3]. Among them, europium-doped lutetium oxide Lu_2O_3:Eu^{3+} is one of the most dense scintillation material (ρ = 9.44 g/sm^3), possessing high X-ray to light conversion efficiency (approximately 80% of CsI:Tl) and high effective atomic number Z_{eff} = 63. Thus only thin layers of Lu_2O_3:Eu^{3+} phosphors are required to complete absorption of X-rays decreasing the multiple scattering of light on the powdered scintillator grains. Sharp emission in the red region of the spectrum (with a maximum at ~611 nm) allows one to use Lu_2O_3:Eu^{3+} screens in combination with a-Si:H and CCD arrays.

Scintillation performance of X-ray screens is known to be greatly influenced by phosphor powder properties, namely crystallinity, dispersity, size and morphology of particles. Nanopowders with spherical particles and low agglomeration degree are required for obtaining of close-packed films with high light yield and negligible light scattering. These nanopowders can be more easily consolidated in 2D close-packed structures, and provide improved

* Corresponding author. Tel.: +38 057 341 0415; fax: +38 057 340 9343.
E-mail address: yavetskiy@isc.kharkov.ua (R.P. Yavetskiy).

0925-8388/$ – see front matter © 2010 Elsevier B.V. All rights reserved.
doi:10.1016/j.jallcom.2010.07.199

scintillation characteristics in comparison with films prepared from powders with undefined morphology. Despite a number of methods were employed to synthesize nanocrystalline Lu_2O_3:Eu^{3+} phosphors [18–23], to our best knowledge there are no reports on Lu_2O_3:Eu^{3+} X-ray screens prepared using nanocrystalline powders. This work presents results on fabrication and characterization of Lu_2O_3:Eu^{3+} close-packed films based on nanopowders obtained by different wet chemical methods.

2. Experimental

2.1. Synthesis of Lu_2O_3:Eu^{3+} nanopowders

The precursors were produced via direct strike co-precipitation method from lutetium and europium metal nitrates using oxalic acid ($H_2C_2O_4$, OA), ammonium hydrogen carbonate (NH_4HCO_3, AHC) and urea ($(NH_2)_2CO$) as precipitants. Commercial high-purity oxides (Lu_2O_3, 99.995%, Stanford Materials Corp., and Eu_2O_3, 99.99%, Aldrich-APL) were dissolved in concentrated nitric acid with subsequent evaporation of acid excess. The europium content was 5 at.% with respect to lutetium in all the experiments. Typically, 0.1 M $Lu_{1.95}Eu_{0.05}O_3$ diluted solution was prepared by dissolving of nitrate mixture in deionized water. Then 1 M NH_4HCO_3 or 0.6 M $H_2C_2O_4$ solution was added to the rare earth mother solution under constant stirring to form precipitant. The precipitation was carried out at room temperature; the drip rate was 2 ml/min. For urea homogeneous precipitation, the urea solution was added to 0.5 M mixed rare earth solution (Lu^{3+}/urea molar ratio was 5×10^{-4}). After being homogenized under constant stirring for 2 h, the mixture was heated to 90 °C. After reacting at 90 ± 1 °C for 2 h, the suspension was cooled down to room temperature. Then, the precipitant was aged for 24 h, washed several times with deionized water and ethanol, and dried in air at 25 °C for two days. To obtain Lu_2O_3:Eu^{3+} nanocrystalline powders the precursor was finally calcined at 1200 °C for 2 h in an air atmosphere.

2.2. Film preparation and characterization

Close-packed Lu_2O_3:Eu^{3+} films on glass substrates were obtained by painting technique that is traditionally applied for photographic film formation [24]. The metal patterns were used to prepare films with dimensions of 5 mm × 5 mm, 20 mm × 20 mm, 50 mm × 50 mm and selected thickness in 20–200 μm range. The solution of nitrocellulose in butyl acetate (5%) was used as a binder. The oxide/polymer ratios in the obtained films were 35/65, 50/50 and 80/20 by weight.

The morphology of initial nanopowders and morphology of Lu_2O_3:Eu^{3+} films formed were studied by means of scanning electron microscopy (SEM) with a JSM-6390 LV (JEOL, Japan) and transmission electron microscopy (TEM) using a TEM-125 (SELMI, Ukraine) microscope. The film thickness was determined from the SEM data. The X-ray diffraction (XRD) of the powder was examined on a DRON-2.0 diffractometer (Fe Kα radiation, λ = 1.93728 Å). The X-ray luminescence spectra of Lu_2O_3:Eu^{3+} nanopowders and films were obtained by SDL-2 (LOMO, Russia) automatic complex. Luminescence was excited by a REIS-E X-ray source (Cu-anticathode deceleration radiation with the energy $E \sim 30$ keV), operating at $U = 30$ kV and $I = 30$ μA. For radioluminescence measurements, the nanopowders were compacted in one batch in pellets of 10 mm in diameter under pressure of 100 MPa. Radioluminescence spectra were measured in the transmission geometry. The X-ray luminescence homogeneity over the film flat area was analyzed using a "Kristall" stand with W-anticathode, $U = 90$, 110 kV, $I \approx 70$ μA.

3. Results and discussion

3.1. SEM and TEM observations of obtained Lu_2O_3 powders

Wet chemical methods are known to produce particles with highly homogeneous distribution of activator ions. The morphology of nanocrystalline particles strongly depends on the precipitant type [25]. Lu_2O_3:Eu^{3+} ($C_{Eu} = 5$ at.%) powders obtained through different wet chemical routes demonstrate different morphological features after calcination. Fig. 1 shows the SEM picture of Lu_2O_3:Eu^{3+} powders prepared with OA, AHC and urea as precipitants. All powders were calcined at $T = 1200$ °C in order to obtain the highest luminescence yield [18]. The temperature of 1200 °C was chosen because it is the upper limit of morphological stability of AHC and urea-precipitated Lu_2O_3:Eu^{3+} powders. Annealing of the powders at higher temperature, despite increase of luminescence yield, results in sintering of adjacent particles together that substantially reduces the particles packing density. Lu_2O_3:Eu^{3+}

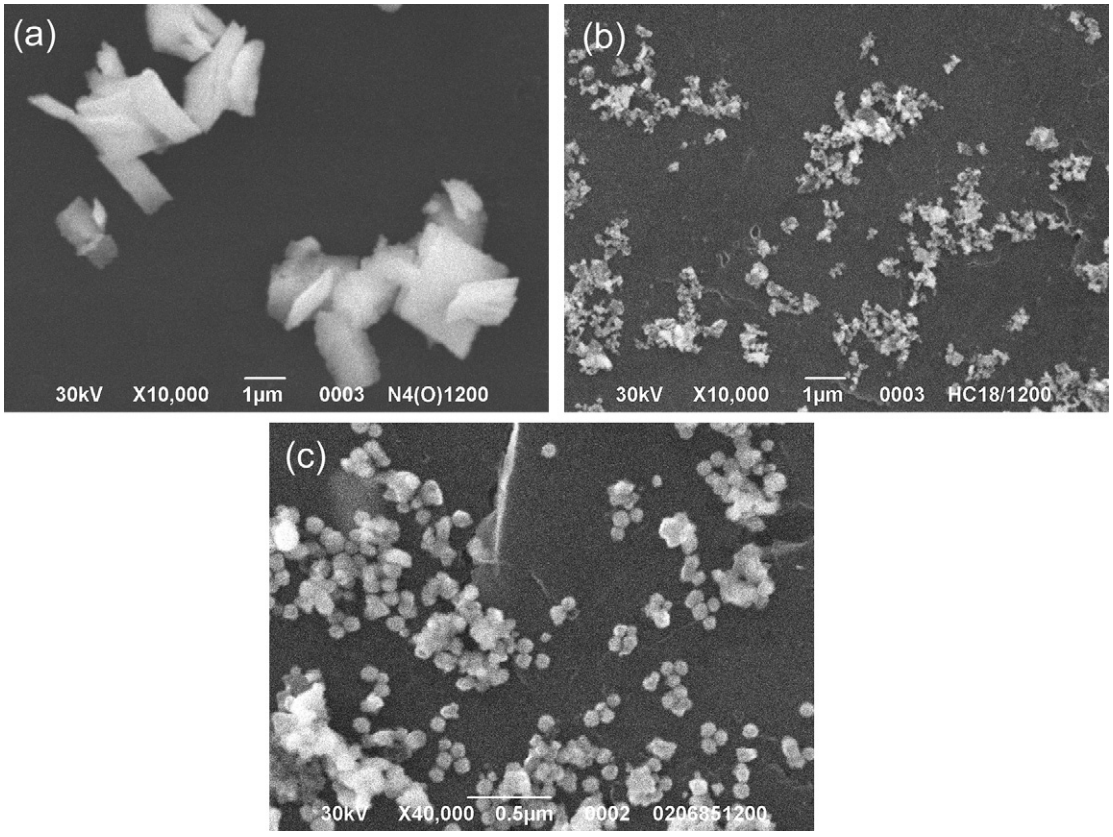

Fig. 1. SEM images of Lu_2O_3:Eu^{3+} nanopowders obtained with $H_2C_2O_4$ (a), NH_4HCO_3 (b) and $(NH_2)_2CO$ (c) as precipitants after calcination at 1200 °C for 2 h.

powders obtained with oxalic acid consist of plate-like aggregates with average size of 1–3 μm (Fig. 1a). It is hard to distinguish by SEM the size of primary crystallites forming each plate. Powders produced by AHC are more dispersed and only slightly agglomerated (Fig. 1b). The particle size determined by SEM is of about 100 nm. The optimization of homogeneous precipitation conditions [18] allows one to obtain near-monodisperse Lu_2O_3:Eu^{3+} crystalline spheres (10% of standard deviation in size distribution) of 100 nm in diameter (Fig. 1c). The particles do not agglomerate, because the relatively high synthesis temperature of precursor provides thermal agitation in the reaction mixture and promotes destruction of the bonds between particles. However, calcination at 1200 °C which is required for maintaining of high luminescence yield, results in little aggregation and loss of ideal spherical morphology due to sintering of adjacent particles. Despite this fact, Lu_2O_3:Eu^{3+} powders produced by urea precipitation have the most favorable morphological characteristics for creation of close-packed homogeneous films. Obviously, the utilization of monodisperse nanospheres provides more uniform packing of the particles in the film and higher density in comparison with nanopowders with irregular morphology. The higher packing density, the lower film thickness is required to absorb X-ray radiation; consequently, the higher spatial resolution can be obtained.

Fig. 2 shows TEM images of Lu_2O_3:Eu^{3+} powders precipitated by AHC. Particles have near spherical form and diameter of about 100–150 nm in the good agreement with SEM data (Fig. 1b). The selected area diffraction (SAED) pattern in Fig. 2b corresponding to diffraction from several Lu_2O_3:Eu^{3+} particles (shown in Fig. 2a) demonstrates only individual point reflections. This indicates that each particle is a single crystal.

3.2. X-ray diffraction analysis of Lu_2O_3:Eu^{3+} powders

The crystalline structure of the powders was investigated by XRD analysis. All the powders obtained belong to well-formed cubic Lu_2O_3 structure reported in the standard JCPDS card 12-0728. Lu_2O_3:Eu^{3+} lattice parameters calculated for the all powders studied are slightly higher than that for undoped Lu_2O_3 due to isomorphous substitution of Lu^{3+} (ionic radius 0.84 Å) by the bigger Eu^{3+} ion (ionic radius 0.96 Å) [26]. The diffraction peak widths give information about the size of crystallites in Lu_2O_3:Eu^{3+} powders. The average crystallite size (L) of powders was calculated from XRD line broadening with the Sherrer's formula. The crystallite sizes determined for OA, AHC and urea-derived powders are 80.5, 71.5 and 107 nm, correspondingly. The huge difference between particle size determined by SEM and crystallite size determined by XRD methods for OA particles means that every micron-sized particle observed by SEM is a dense aggregate of nano-sized primary particles. The observed differences in the crystallite size can be related to different decomposition temperatures of each precursor used. The highest L value obtained for urea-precipitated nanopowders evidences the better crystallinity of particles and is favorable to obtain better luminescent properties. The average crystallite size of Lu_2O_3:Eu^{3+} nanopowders precipitated by urea is comparable to the particle size determined by SEM, that indicates the perfect crystalline structure.

3.3. Lu_2O_3:Eu^{3+} films characterization

Previously grinded Lu_2O_3:Eu^{3+} powders mixed with nitrocellulose solution in butyl acetate were used for film preparation. Smooth homogeneous Lu_2O_3:Eu^{3+} films of different sizes and thickness in 20–200 μm range were obtained by painting technique. The compositions of Lu_2O_3:Eu^{3+}/polymer were 35/65, 50/50 and 80/20 by weight. Fig. 3 presents the typical SEM images of film surfaces obtained using different Lu_2O_3:Eu^{3+} powders. The films

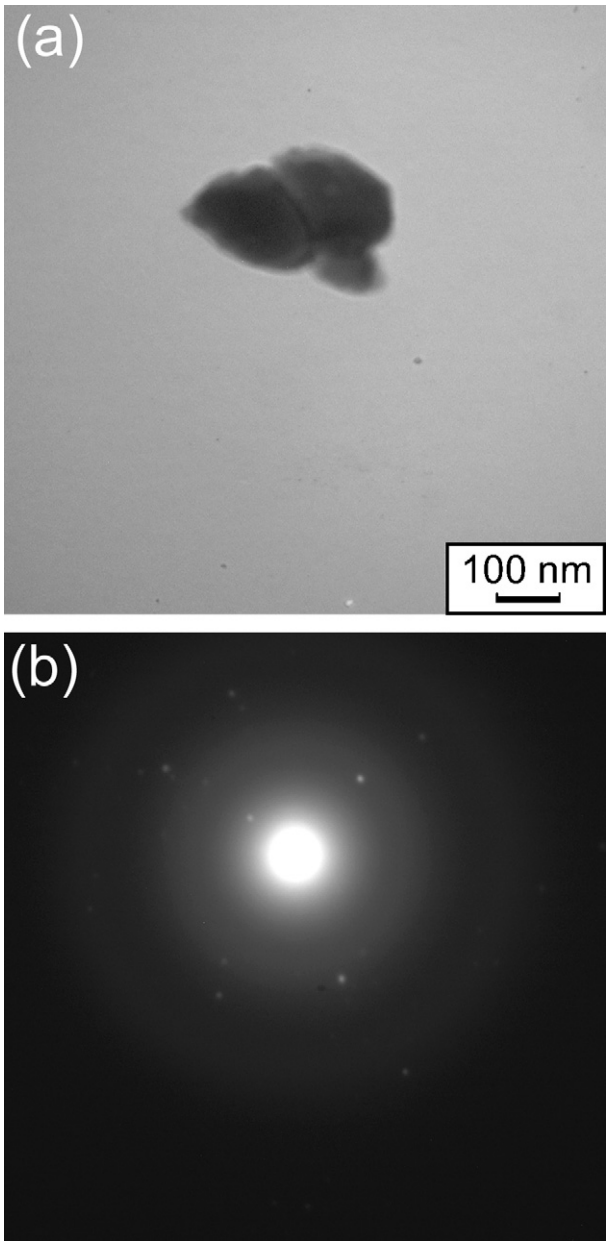

Fig. 2. TEM image of Lu_2O_3:Eu^{3+} nanopowders obtained with NH_4HCO_3 (a) and SAED pattern from the several particles (b).

thickness is 200 μm, size 20 mm × 20 mm and Lu_2O_3:Eu^{3+}/polymer ratio is 80/20. SEM reveals that morphology of initial nanoparticles generally retains in films deposited on the glass substrate. As one can see, the relatively simple and low cost painting technique permits to control the size and the thickness of phosphor layer on the substrate and provides fabrication of uniform and close-packed Lu_2O_3:Eu^{3+} films. The films prepared from much concentrated suspension (Lu_2O_3:Eu^{3+}/polymer weight ration of 80/20) have higher density essential to better scintillation efficiency.

Lu_2O_3:Eu^{3+} nanopowders with different morphology were coated onto glass substrate to form smooth homogeneous films. The relative density of Lu_2O_3:Eu^{3+} films studied was estimated by geometrical method. That means film density is equal to mass/volume ratio (the film thickness was estimated from SEM data). For 20 μm coated phosphor films, the packing densities were 60 ± 2, 50 ± 2 and 68 ± 2% for OA, AHC and urea-precipitated Lu_2O_3:Eu^{3+} nanopowders. This result correlates with morphological peculiarities of Lu_2O_3:Eu^{3+} nanopowders. Spherical, smooth,

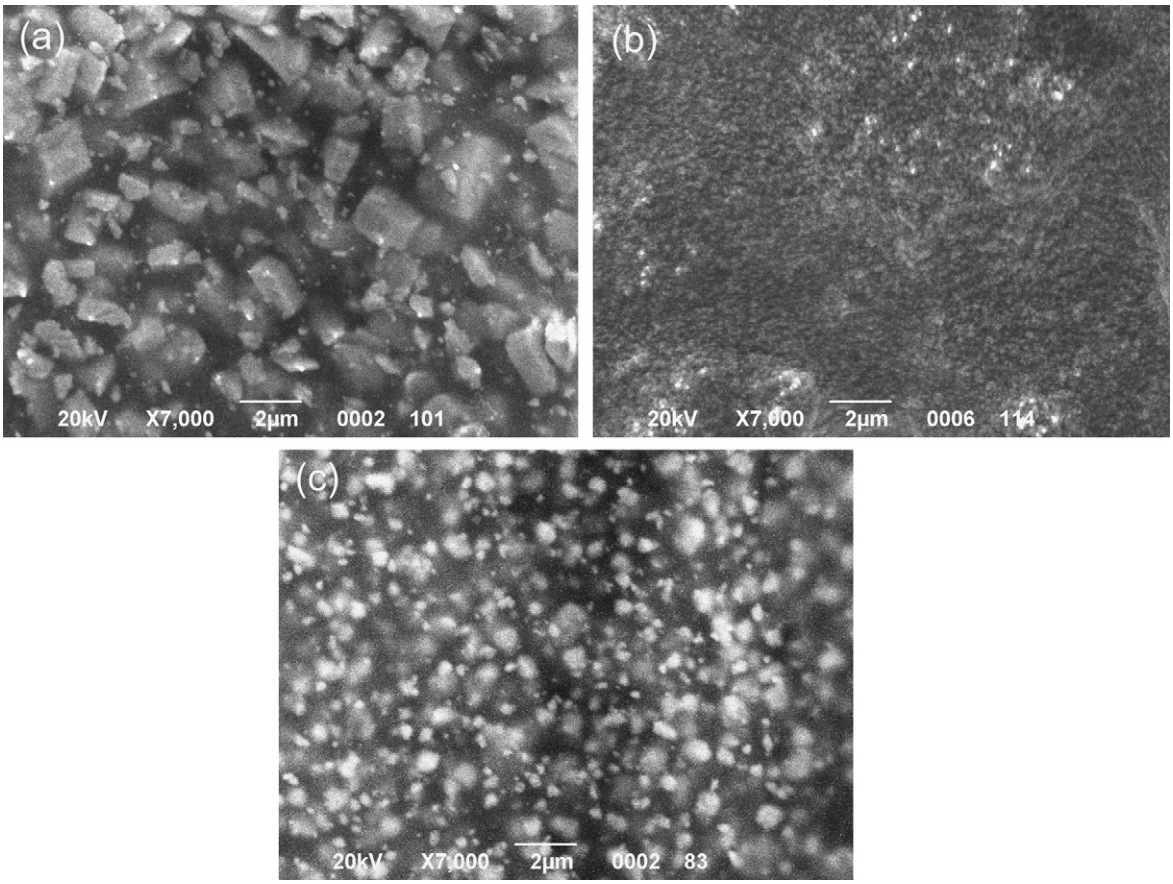

Fig. 3. The morphology of films surfaces obtained from Lu_2O_3:Eu^{3+} powders precipitated by $H_2C_2O_4$ (a), NH_4HCO_3 (b) and $(NH_2)_2CO$ (c).

and non-agglomerated particles with narrow size distribution are necessary for preparation of close-packed high-filled films. The highest density value of 68% obtained with Lu_2O_3:Eu^{3+} urea-derived nanoparticles is higher than theoretical one for random close-packed spheres (that is, 64% density) [27]. The micron-sized particles (produced with AO) also form dense film, probably, due to low specific surface area and, consequently, low interaction of particles in suspension. The aggregated nanopowders produced with AHC have the lowest packing density due to agglomeration of initial phosphor powder. The fine powder cause huge friction forces between particles during deposition, which impede formation of dense homogeneous microstructure. Thus, painting technique ensures production of smooth, homogeneous, and close-packed phosphor films with controllable thickness and morphology when fine spherical particles are used.

3.4. *Luminescence of Lu_2O_3:Eu^{3+} films under X-ray excitation*

Luminescence efficiency of scintillation films is a function of many parameters, such as film thickness, density, and a type of the phosphor powder used. The luminescence spectra were measured for all Lu_2O_3:Eu^{3+} powders and films under X-ray excitation. The influence of powder type on luminescence yield of Lu_2O_3:Eu^{3+} was estimated. The luminescent spectra of the powders are similar to the films fabricated from these powders. Therefore, only luminescence spectra of Lu_2O_3:Eu^{3+} films are presented in Fig. 4. They consist of group of lines in $\lambda = 550–750$ nm spectral region corresponding to $^5D_0 \rightarrow {}^7F_J$, ($J = 0–4$) transitions of Eu^{3+} ions. The $^5D_0 \rightarrow {}^7F_2$ electric dipole hypersensitive transition with the maximum at 611 nm is dominant. The emission spectrum of Lu_2O_3:Eu^{3+} coincides better with the spectral sensitivity characteristics of CCD arrays, as compared to commercial GOS:Tb^{3+}. This means that light produced with Lu_2O_3:Eu^{3+} scintillator can be more effectively registered by detection system. The urea-precipitated coated nanophosphors possess higher scintillation yield, compared to AHC and OA phosphor films. This is attributed to spherical form, absence of particles agglomeration and higher packing density of urea-derived phosphor films (Fig. 4c). Additionally, spherical form of the phosphor particles minimizes light scattering effect on the film sur-

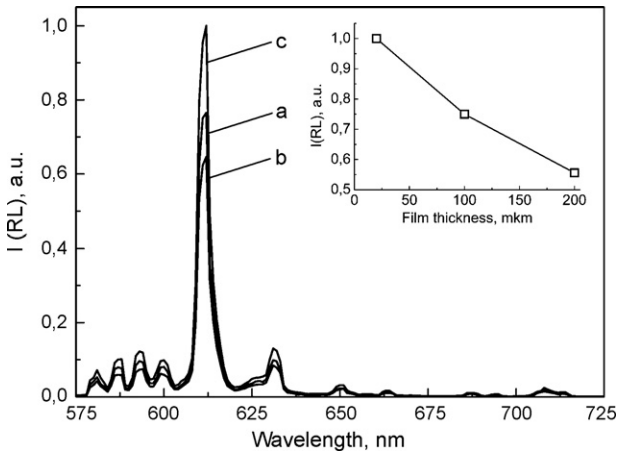

Fig. 4. Normalized room-temperature X-ray luminescence spectra of Lu_2O_3:Eu^{3+} films obtained from nanopowders precipitated by $H_2C_2O_4$ (a), NH_4HCO_3 (b) and $(NH_2)_2CO$ (c). The inset: Luminescence intensity of Lu_2O_3:Eu^{3+} films (c) vs. their thickness.

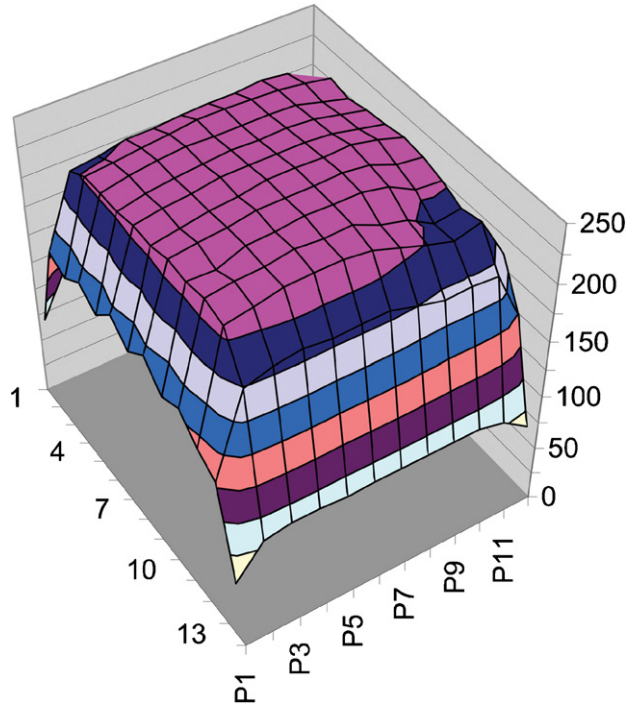

Fig. 5. The topogram of X-ray luminescence intensity of Lu_2O_3:Eu^{3+} screen obtained using 100 nm spheres.

face. High degree of agglomeration and non-spherical form lead to decrease luminescence intensity (Fig. 4a and b). Light output of the screens significantly depends on size of particles in the powder. Typically, the larger particle sizes, the screens with higher light output are produced. It seems to be surprising that 1–3 micron-sized Lu_2O_3:Eu^{3+} powders demonstrate lower scintillation yield compared to 100 nm nanopowder. However, XRD data show that OA produced phosphor particles consist of primary 80 nm crystallites. This size is smaller that for urea-derived nanospheres. Thus, luminescence response of Lu_2O_3:Eu^{3+} screens strictly depends on the primary particle size—the higher crystallite size, the higher scintillation yield is achieved.

The luminescence spectra of Lu_2O_3:Eu^{3+} films obtained from nanospheres with different Lu_2O_3:Eu^{3+}/polymer ratio differs only by integral intensity. The most effective luminescence is observed for high-filled Lu_2O_3:Eu^{3+} film with the Lu_2O_3:Eu^{3+}/polymer ratio of 80/20. Increase of the polymer content leads to decrease of packing density and luminescence intensity. The same behavior was found for all types of nanopowders. Thus Lu_2O_3:Eu^{3+}/polymer ratio of 80/20 is optimal to obtain Lu_2O_3:Eu^{3+} film with high scintillation yield. The fabricated films with different phosphor/polymer ratio were not heat-treated, because heat treatment can lead to decrease of film adhesion to substrate. Thus luminescent properties of films can be influenced by polymer, which can reduce luminescent intensity for the film with lower phosphor/polymer ratio. However, organic binder in high-filled luminescent films protects the phosphor particles from interaction with air atmosphere without significant lowering of scintillation response. Luminescence efficiency and spatial resolution of screens also depends on their thickness. Different detector application requires different phosphor layers thicknesses. Fig. 3, inset, presents the dependence of Lu_2O_3:Eu^{3+} films luminescence intensity on their thickness. It was shown that for all types of powders film thickness decrease promotes luminescence increase. The thicker the film, the less light it transfers to the detection system. Therefore, Lu_2O_3:Eu^{3+} films with 20 μm thickness and Lu_2O_3:Eu^{3+}/polymer ratio of 80/20 are more effective for high-resolution X-ray scintillation screens.

Uniform distribution of phosphor particles in the film volume is essential for the preparation of highly efficient scintillation screen. Homogeneity of X-ray luminescence intensity over the film area is a crucial parameter for testing the scintillation material. Fig. 5 presents the representative distribution of X-ray intensity obtained with Lu_2O_3:Eu^{3+} urea-derived phosphor film. The topogram demonstrates that profitable structural and morphological features of phosphor particles promote effective X-ray luminescence as well as homogeneous distribution of luminescence intensity over the film flat area.

4. Conclusions

The close-packed scintillation films based on Lu_2O_3:Eu^{3+} powders with different morphology were fabricated by painting technique. The influence of morphology, composition and film thickness on X-ray luminescence intensity was studied. It was shown that 20 μm thick screens with Lu_2O_3:Eu^{3+}/polymer ratio of 80/20 produced from urea-derived nanophosphors show the most efficient X-ray luminescence. Homogeneous distribution of X-ray intensity over the Lu_2O_3:Eu^{3+} film area makes this film a potential candidate for creation of efficient high-resolution scintillation detectors of X-rays.

Acknowledgments

The experimental assistance by Dr. V.N. Baumer, Dr. S.N. Galkin and Dr. O.M. Vovk are greatly acknowledged. Some of the authors (R.P. Yavetskiy and N.V. Babayevskaya) are grateful for financial assistance of NAS of Ukraine through the grant for young scientists under contract No. A/8-09 from July 01, 2009. Fruitful suggestions of Journal Editor Prof. Hongge Pan and reviewers are greatly acknowledged.

References

[1] P. Yu, A. Wu, L. Su, X. Guo, Y.B. Wang, H. Zhao, Y. Yang, Q. Yang, J. Xu, J. Alloys Compd. 503 (2010) 380–383.
[2] H. Feng, D. Ding, H. Li, S. Lu, S. Pan, X. Chen, G. Ren, J. Alloys Compd. 489 (2010) 645–649.
[3] Y. Shi, Q.W. Chen, J.L. Shi, Opt. Mater. 31 (2009) 729–733.
[4] A. Fukabori, T. Yanagida, J. Pejchal, S. Maeo, Y. Yokota, A. Yoshikawa, T. Ikegami, F. Moretti, K. Kamada, J. Appl. Phys. 107 (2010) 073501.
[5] S.R. Podowitz, R. Gaume, R.S. Feigelson, J. Am. Ceram. Soc. 93 (2010) 82–88.
[6] M. Kucera, K. Nitsch, M. Nikl, M. Hanus, S. Danis, J. Cryst. Growth 312 (2010) 1538–1545.
[7] P. Horodysky, J. Tous, K. Blazek, M. Nikl, Yu. Zorenko, M. Kucera, Radiat. Meas. 45 (2010) 628–630.
[8] A. Cecilia, et al., Nucl. Instrum. Methods Phys. Res. Sect. A (2010), doi:10.1016/j.nima.2010.06.192.
[9] A.deJ. Morales Ramírez, A. García Murillo, F.deJ. Carrillo Romo, J. Ramírez Salgado, C. Le Luyer, G. Chadeyron, D. Boyer, J. Moreno Palmerin, Thin Solid Films 517 (2009) 6753–6758.
[10] A. Garcia Murillo, F.deJ. Carrillo Romo, C. Le Luyer, A.deJ. Morales Ramirez, M. Garcia Hernandez, J. Moreno Palmerin, J. Sol–Gel Sci. Technol. 50 (2009) 359–367.
[11] M. Gu, L. Zhu, X. Liu, S. Huang, B. Liu, C. Ni, J. Alloys Compd. 501 (2010) 371–374.
[12] G. Fern, T. Ireland, J. Silver, R. Withnall, A. Michette, C. McFaul, S. Pfauntsch, Nucl. Instrum. Methods Phys. Res. Sect. A 600 (2009) 434–439.
[13] H.H.S. Oliveira, M.A. Cebim, A.A. DaSilva, M.R. Davolos, J. Alloys Compd. 488 (2009) 619–623.
[14] Y. Wang, Q. He, B. Chu, J. Alloys Compd. 479 (2009) 704–706.
[15] M. Gu, L. Jia, X. Liu, S. Huang, B. Liu, C. Ni, J. Alloys Compd. 502 (2010) 190–194.
[16] E.-J. Popovici, M. Nazarov, L. Muresan, D.Y. Noh, L.B. Tudoran, E. Bica, E. Indrea, J. Alloys Compd. 497 (2010) 201–209.
[17] A. Wiatrowska, E. Zych, L. Kępiński, Radiat. Meas. 45 (2010) 493–496.
[18] N.A. Dulina, Yu.V. Yermolayeva, A.V. Tolmachev, Z.P. Sergienko, O.M. Vovk, E.A. Vovk, N.A. Matveevskaya, P.V. Mateychenko, J. Eur. Ceram. Soc. 30 (2010) 1717–1724.
[19] H. Wei, Z. Cleary, S. Park, K. Senevirathne, H. Eilers, J. Alloys Compd. 500 (2010) 96–101.

[20] X. Li, M. Yu, Z. Hou, W. Wang, G. Li, Z. Cheng, R. Chai, J. Lin, J. Colloid Interface Sci. 349 (2010) 166–172.
[21] Ž. Antić, B. Bártová, M.D. Dramićanin, J. Alloys Compd. 505 (2010) 224–228.
[22] D. Zhou, Y.Y. Ren, Y. Shi, J.Y. Xu, G.J. Jiang, J.J. Xie, J. Alloys Compd 504 (2010) L36–L38.
[23] Z. Antic, et al., Opt. Mater. (2010), doi:10.1016/j.optmat.2010.05.022.
[24] S. Biswas, P. Pramanik, P.K. Basu, Mater. Lett. 4 (1986) 81–84.
[25] D. Zhou, Y. Shi, P. Yun, J.J. Xie, J. Alloys Compd. 479 (2009) 870–874.
[26] R. Shannon, Acta Crystallogr. A32 (1979) 751–767.
[27] G.L. Messing, A.J. Stevenson, Science 322 (2008) 383–384.